Available online at www.sciencedirect.com
ScienceDirect
Journal of Sound and Vibration 320 (2009) 527–544
JOURNAL OF SOUND AND VIBRATION
www.elsevier.com/locate/jsvi

# A model for the characterization of friction contacts in turbine blades

M. Allara*

*Department of Mechanical Engineering, Politecnico di Torino, Corso Duca degli Abruzzi 24, 10129 Turin, Italy*

Received 21 August 2007; received in revised form 12 July 2008; accepted 11 August 2008
Handling Editor: M.P. Cartmell
Available online 24 September 2008

**Abstract**

Stresses produced by the forced vibrations can lead to a significant reduction of the life of turbo engine blades. To predict the vibration amplitudes of this components an accurate dynamic analysis is necessary. The forced response calculation of these dynamic systems is strongly affected by the presence of the contact interfaces (i.e., underplatform dampers, shrouds, root joints). Different contact models are available in literature. These models make use of contact parameters, contact stiffness and friction coefficient to evaluate the damping and stiffness related to the contact interfaces. In this paper a model is proposed to characterize friction contact of non-spherical contact geometries obeying the Coulomb friction law with constant friction coefficient and constant normal load. The hysteresis curves of the oscillating tangential contact forces vs. relative tangential displacements and the dissipated energy at the contact are obtained for different contact geometries. The developed model is suitable to be implemented in numerical solvers for the calculation of the forced response of turbine blades with embedded friction contacts.


## 1. Introduction

Stresses produced by resonant vibrations may significantly affect the life of turbo engine blades. A correct design of bladed disks requires the capability to predict the resonance frequencies and the forced response levels. In order to achieve these objectives, knowledge of damping and stiffness related to the different contact interfaces (i.e., underplatform dampers, shrouds, root joints) is fundamental. Such contacts are usually characterized by high contact pressures and a small amplitude of relative displacement. In order to characterize their behaviour, relationships are necessary between the contact forces (tangential and normal) and the corresponding relative displacement at the contact. These relationships are commonly provided in the form of hysteresis cycles of contact forces.

Many papers [1–7] studied the non-linear behaviour of dynamic systems embedding friction contacts. The steady-state forced response of bladed disks is computed by means of the harmonic balance method: the response of the system is assumed harmonic or a superimposition of harmonics and the periodical contact

*Tel.: +39 011 564 6953; fax: +39 011 564 6999.
*E-mail address:* marco.allara@polito.it

0022-460X/$ - see front matter © 2008 Elsevier Ltd. All rights reserved.
doi:10.1016/j.jsv.2008.08.016

forces at the contact interfaces are approximated by a truncated series of harmonic terms. The employed dynamic friction models can simulate very general contact conditions, such as microslip behaviour, stick–slip transition, variable normal load and separation of the interfaces.

The latest and most advanced contact models [8,9] make use of three parameters to characterize the contact behaviour: the friction coefficient, the tangential contact stiffness and the normal contact stiffness. A vast technical literature deals with the problem of the characterization of the above mentioned contact parameters. Several experimental works study the friction coefficient behaviour under variable contact condition: relative velocity and displacement, surface material properties, temperature, adhesion, welding and local contacts, elastic and plastic deformations, wear, oxidation, lubricants, third body. Some papers are addressed to study the friction coefficient for typical turbo engine materials at room temperature [10] and at high temperature [11,12]. Besides different experimental approaches have been used to evaluate the value of the tangential contact stiffness. Experimental measurements of hysteresis curves are presented in Ref. [13] for flat contacts and in Ref. [10] for spherical contacts. In Ref. [6], the stiffness parameters are obtained by means of curve fitting in frequency domain between experimental and numerical frequency response functions. The experimental approach requires that the geometry of the contact interface is known and usually this is not the case in the design stage, moreover the contact stiffness depends on several parameters, geometrical dimensions, material properties, loads, and it is not feasible to obtain a complete experimental characterization. To overcome these difficulties some works propose numerical methods based on finite element models [14–16]. Usually these methods check effectiveness of the contact element parameters and of the mesh refinement by considering the Hertzian contact problem, and then the same method is applied to different and more general contact geometries. As an alternative to numerical FE simulations, the analytical approach, based on the continuum contact mechanics, has been used only for the Hertzian spherical contacts. For such a contact geometry the hysteresis curves can be obtained analytically in close form [17,18]. In the field of turbine blade vibration, Mindlin's theory has been applied in Refs. [19,20] to predict the behaviour of an underplatform friction damper with spherical contacts. These papers by Koh et al. show that continuum mechanics can be usefully applied to estimate the dynamic behaviour of friction interfaces. However common contact geometries in real bladed discs components are not spherical, but flat or cylindrical with one side of the contact area, referred as $L$ in Fig. 1a, significantly wider than the other.

In the literature, several contact models have been developed to define analytically the normal and shear stress fields around friction contacts. In these works, the problem of two bodies in contact is studied with the theory of one body (i.e., cylinder, flat punch, etc.) pressed against an infinite half-plane using 2D elasticity theory. The main drawback of this approach is that the relative displacements of the bodies in contact cannot be computed. In detail, if $r$ is the distance of a point $P$ from the contact surface, as $r$ tends to infinity the displacements in $P$ are of the order of $\ln(r)$ and go to infinity too. On the contrary, in 3D elasticity theory the displacements of a point $P$ are of the order of $1/r$, and so, as $r$ tends to infinity, the displacements go to zero [21]. As a consequence, hysteresis curves of tangential and normal contact forces cannot be computed with 2D contacts models, and these models cannot be used to characterize the contact interfaces of turbine blades with the aim of predicting the corresponding damping and stiffness. In order to find the value of the displacements it is necessary to discard the 2D assumptions and take into account the full geometry of the contact bodies.

In this paper a model is proposed to characterize friction contact of non-spherical bodies and to compute the hysteresis curves of tangential contact forces vs. relative tangential displacements. The aim of the paper is to provide a simple and effective method to estimate the effect of the main contact parameters (contact geometry, material properties, loads) on the contact behaviour.

The proposed model is based on the following steps:

1. The friction contact is simulated by a 3D flat indenter with rounded edges pressed against an infinite half-plane (Fig. 1b).
2. The normal and shear stress distributions of a 2D flat indenter with rounded edges over an infinite half-plane are analytically computed by means of the contact model developed by Ciavarella et al. [22].
3. The 2D solution obtained at step 2 is extended to the 3D geometry with the assumption that neither pressure nor shear stress vary along the contact area length.

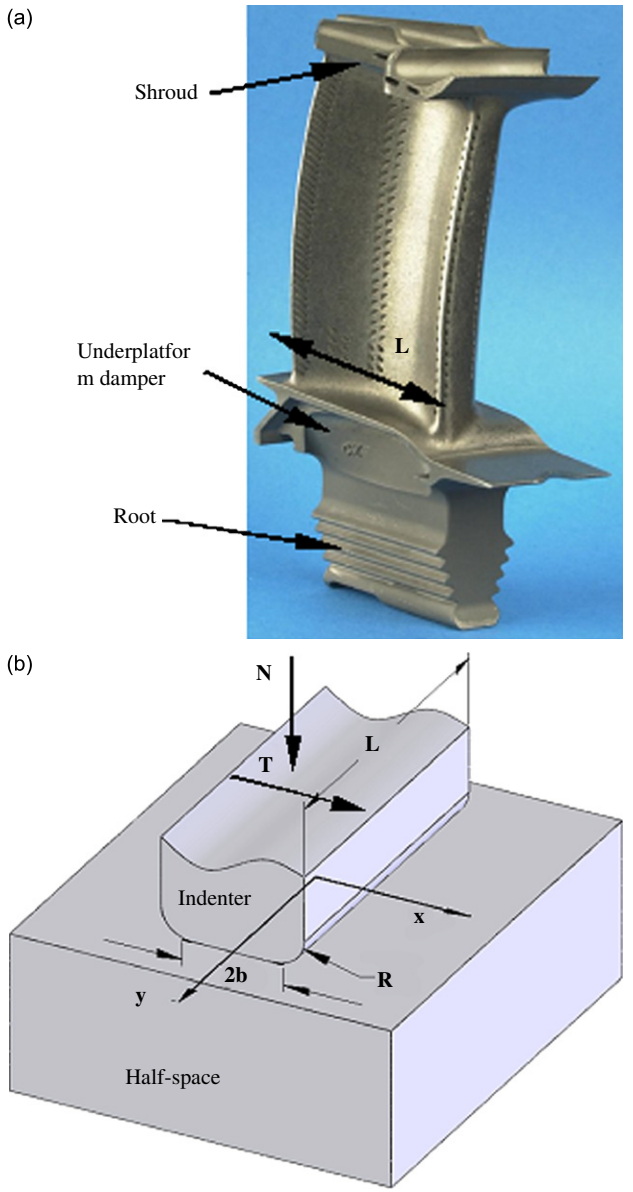


Fig. 1. (a) Real contact configurations and (b) simplified contact problem: normal ($N$) and tangential ($T$) load applied to the contact.

4. The resulting 3D pressure and shear stress distributions are used to compute the relative displacements of the contact surfaces by means of the Cerruti potential theory [23].
5. Steps 1–4 are repeated for different values of tangential load in order to compute the monotonic loading curve of the tangential contact force vs. the tangential contact displacement up to gross-slip conditions.
6. The periodic hysteresis curve is obtained from the monotonic curve computed at step 5 by means of the Masing rule [24,25]. These hysteresis curves can be implemented in the numerical solvers based on the harmonic balance method to compute the forced response of turbine blades with friction contacts.

Normal and shear stress distributions computed at step 2, which represent the fundamental input of the model, are computed under the hypothesis of constant normal load acting at the contact. Therefore, in case of contacts where the variation of the normal load is negligible with respect to the superimposed static normal load (i.e., for blade roots and some shrouds) the model can be directly implemented in a non-linear numerical solver.

## 2. Contact model

### 2.1. Hypotheses

The model proposed in this paper is based on the following hypotheses:

1. Perfectly isotropic and elastic materials of the bodies in contact.
2. Perfectly smooth contact surfaces (i.e., surface roughness is not taken into account).
3. The complex geometry of contact interfaces (Fig. 1a) modelled by the contact of a 3D flat indenter with rounded edges on a half-space (Fig. 1b).
4. Rectangular contact area (Fig. 1b) with large aspect ratio (i.e., length $L$ much greater than the half-width $b$).
5. The two bodies in contact considered as half-planes. This assumption is certainly justified when the ratio between the half-width of the contact area and the radius of curvature, $b/R$, is small. Actually the outer parts of the indenter will support the contact area in the same way as for the Hertzian case. As the contact patch extends further into the curved region the half-space assumption becomes poorer and the overall geometry becomes increasingly more important.
6. Friction contact characterized by 1D tangential relative displacements along the contact width (Fig. 1b) and Coulomb's friction law with constant friction coefficient, $\mu$, assumed to be known.
7. Constant normal load at the contact (i.e., the variation of normal load due to vibrations is negligible in comparison with the superimposed static normal load). This hypothesis is requested to simplify the construction of the hysteresis curves; however, it is not strictly necessary as it is shown in Ref. [26] even if the analytical treatment becomes so complicate that a purely numerical approach can be preferred.

### 2.2. The 2D pressure and shear traction distributions

The first step of the proposed methodology is the calculation of pressure and shear stress distribution over the contact area of a flat indenter pressed against a half-space.

Analytical solutions for the 3D problems do not exist. On the contrary a 2D analytical solution has been provided in Ref. [22]. Such a solution is based on the assumption that the two bodies in contact have the same elastic constants [21], otherwise the resulting system is made of coupled balance equations and the exact analytical solution is not known. However the coupling effect is generally small [27] and in many real applications the bodies in contact are of the same material.

The detailed description of the theory can be found in the reference papers [21,22]. The final governing equations are reported in Appendix A and only the main results are here described (Fig. 2).

The examined geometry is shown in Fig. 3, a flat indenter with rounded edges with $a$ the half-width of the straight part of the punch and $b$ the half-width of the contact area after the application of the normal load. For this geometry the non-dimensional pressure distribution $p(x)$ plotted in Fig. 3 depends only on the ratio $a/b$, that can be evaluated by means of the equation

$$\frac{4PR}{a^2E^*} = \frac{\pi - 2\varphi_0}{2\sin^2\varphi_0} - \cot(\varphi_0) \tag{1}$$

where $a/b = \sin\varphi_0$ is unknown. $P$ is the normal load for unit of length equal to the whole normal load, $N$, divided by the length of the contact, $L$, $R$ the radius of curvature, $a$ the semi-width of the flat part and $E^*$ a measure of the composite stiffness of the two bodies in contact, defined under plain strain conditions by

$$\frac{1}{E^*} = \frac{1}{E_1}(1 - \nu_1^2) + \frac{1}{E_2}(1 - \nu_2^2) \tag{2}$$

with $E_i$ as the Young's modulus and $\nu_i$ the Poisson's ratio of body $i$.

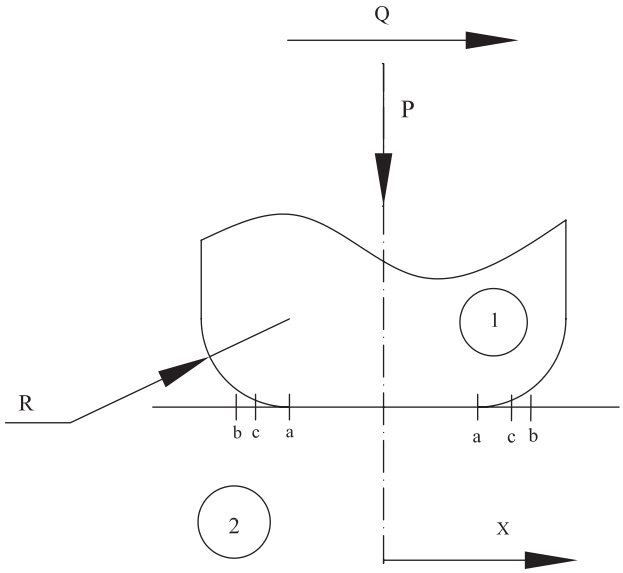


Fig. 2. Flat punch with rounded edges. $P$: normal load for unit of length, $Q$: tangential load for unit of length, $a$: half-width of the flat part, $c$: half-width of the central stick area, $b$: half-width of the contact area, $R$: radius of curvature.

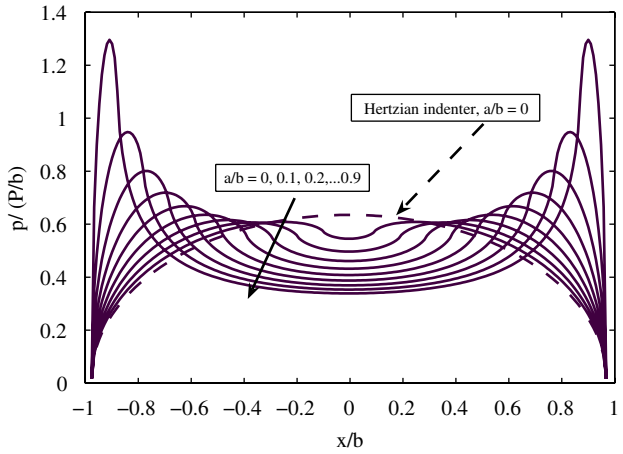


Fig. 3. Non-dimensional pressure distributions for different values of the ratio $a/b$. For $a/b = 0$ the solution for the Hertzian parabolic indenter is obtained.

As pointed out in Ref. [22], the parameter $g = 4PR/a^2E^*$ can vary from zero to infinite as a function of the contact parameters: geometry, $R$ and/or $a$, material properties, $E^*$ or normal load, $P$. When $g$ vanishes the indenter tends to a flat pad indenter with sharp edges, on the other hand, if $g$ tends to infinity, the shape of the geometry tends to a Hertzian cylindrical indenter. Therefore the Hertzian cylindrical indenter can be analysed as a special case of the flat with rounded edges solution.

The shear traction distribution $q(x)$, for a given constant normal load, is provided in Ref. [22] and here reported in Fig. 4 for different values of tangential force applied to the contact. If $Q/\mu P < 1$ microslip occurs at the edges of the contact region, for $c \leqslant |x| \leqslant b$, being $c$ the half-width of the stick zone where microslips of the contact points is not allowed (Fig. 2). When $Q/\mu P = 1$ the whole contact area can slip and gross slip occurs. The model always predicts microslip at the edges of the contact area, even for very low ratio of $Q/\mu N$. If no slip is allowed the ratio of shear to normal tractions, $q(x)/p(x)$, approaches infinity as $x$ approaches the edges of the contact and an infinite coefficient of friction will be required to prevent slips at the edges [28].

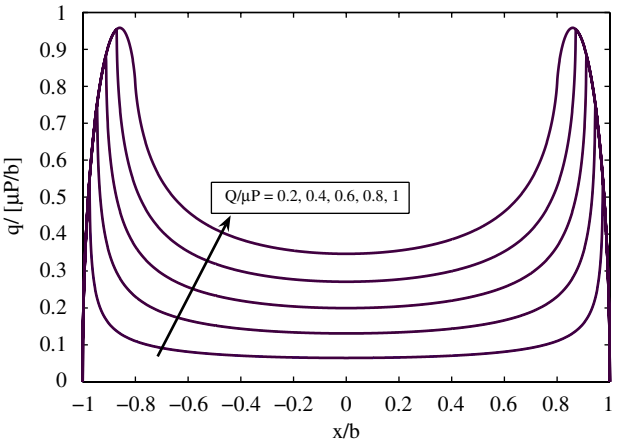


Fig. 4. Non-dimensional shear traction distribution for a given ratio $a/b$ and different ratio $Q/\mu P$.

This feature is typical of incomplete contact where the contact pressure falls continuously to zero toward the edges of the contact. A typical example is Mindlin's solution [17].

The pressure and shear traction distributions obtained in this section are used in the next paragraph as starting point to derive the hysteresis curves of the tangential force vs. the relative tangential displacement.

### 2.3. Relationship between tangential force and tangential displacement

The solutions reported in the previous paragraph are very effective to study fretting fatigue contact problems or fatigue crack propagation. However, they cannot be directly used to determine the hysteresis curves of the tangential force vs. the relative tangential displacement which characterize the dynamic behaviour of the contact interface.

In this paragraph a method is described to obtain a relationship between the tangential force and the tangential displacement, to be used to compute the hysteresis curves, when the 3D pressure and shear stress distribution are known, then it will be shown below that.

Abandoning the 2D assumption and turning to a 3D contact problem, the classical approach to obtain the displacements caused by a surface traction distribution applied upon a half-space is due to Cerruti and Bussinesq who developed the potential theory. By means of these results, it is possible to obtain a useful set of equations relating the shear traction distribution, previously obtained, to the complete displacement field. As it was before pointed out, under the simplifying hypothesis of bodies elastically similar, normal and tangential problem becomes uncoupled and the influence of normal pressure and shear traction can be examined separately.

If a half space is subjected to a distributed shear traction, $q_x$ in Fig. 5, the resulting displacements [28] are

$$u_x = \frac{(1+v)}{2\pi E}\int\int q_x(r,s)\left[\frac{1}{R}+\frac{1-2v}{R+z}+\frac{(r-x)^2}{R^3}-\frac{(1-2v)(r-x)^2}{R(R+z)^2}\right]\mathrm{d}r\,\mathrm{d}s$$

$$u_y = \frac{(1+v)}{2\pi E}\int\int q_x(r,s)\left[\frac{(r-x)(s-y)}{R^3}-\frac{(1-2v)(r-x)(s-y)}{R(R+z)^2}\right]\mathrm{d}r\,\mathrm{d}s$$

$$u_z = -\frac{(1+v)}{2\pi E}\int\int q_x(r,s)\left[\frac{(r-x)z}{R^3}-(1-2v)\frac{(r-x)}{R(R+z)}\right]\mathrm{d}r\,\mathrm{d}s \tag{3}$$

where

$$R^2 = (x-r)^2+(y-s)^2+z^2 \tag{4}$$

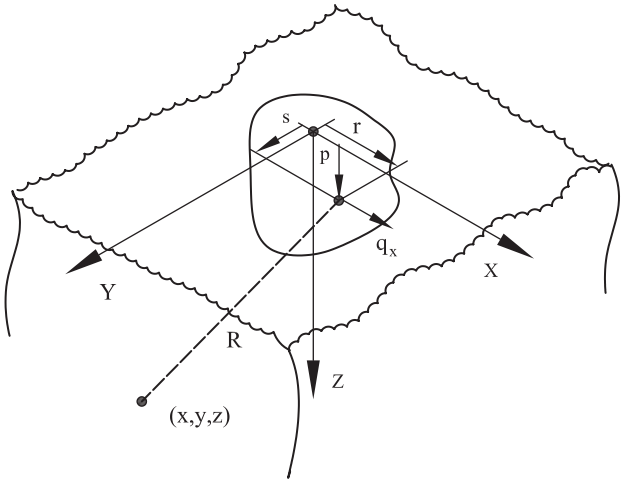


Fig. 5. A half-space $z>0$ subject to a distributed traction over a certain region. Elements of traction, $p$, $q_x$, located at $(r, s)$ and a general point $(x, y, z)$ where displacements can be evaluated by means of Cerruti potential equations.

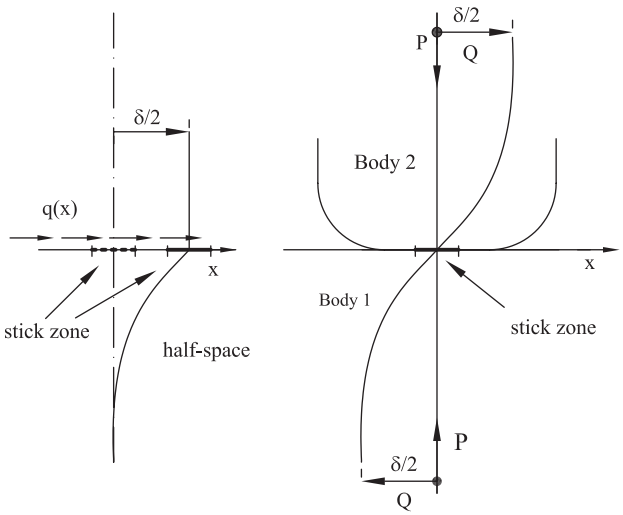


Fig. 6. Displacement of the stick area on a half-space and rigid-body displacement of distant points in two bodies in contact.

Since in the case under study the relative displacement at the contact is supposed to be 1D and along the $x$ direction of Fig. 2, only the first of Eq. (3), referred to $u_x$, is hence considered.

The displacement is evaluated in the centre of the contact area, i.e., in the centre of the stick zone, because this is the last point to remain stuck to the other contact body before that global slip occurs. This displacement can be thought of both as the displacement of the stick area with respect to fixed points distant from the contact surface and the rigid-body displacement of the distant points in the far field with respect to the stick area, assumed motionless (Fig. 6). Indeed, differently from 2D contact problems, in 3D problems the relative displacement between the contacting bodies approaches a finite limit in the far field and consequently the value of the contact stiffness is uniquely defined, as it is also pointed out in Ref. [19]. The same approach is provided both by classical works [17] and more recent papers [29].

To obtain the displacement $u_x$ on the centre of the contact, the integral equation must be evaluated in $x = y = z = 0$. By this substitution the previous equation becomes

$$u_x = \frac{(1+\nu)}{2\pi E} \int\int q_x(r,s) \left[ \frac{2-2\nu}{R} + \frac{2\nu r^2}{R^3} \right] \mathrm{d}r\, \mathrm{d}s \tag{5}$$

In order to apply Eq. (5) to the case of the 3D flat indenter with rounded edges under study in this paper, it is here assumed that the distribution of shear stress $q(x)$ computed with the 2D contact model of Ref. [22] and plotted in Fig. 4, is constant along the indenter length $L$. Therefore, Eq. (5) becomes

$$u_x = \frac{(1+v)}{\pi E}\int_{-b}^{b} q_x(r)\int_{-L/2}^{L/2}\left[\frac{(1-v)}{\sqrt{r^2+s^2}}+\frac{vr^2}{(r^2+s^2)^{3/2}}\right]\mathrm{d}s\,\mathrm{d}r \tag{6}$$

where the integral is computed over the contact rectangular area of length $L$ and half-width $b$.

The inner integral becomes

$$2\int_0^{L/2}\left[\frac{(1-v)}{\sqrt{r^2+s^2}}+\frac{vr^2}{(r^2+s^2)^{3/2}}\right]\mathrm{d}s = 2\left[(1-v)\,\ln[s+(r^2+s^2)^{1/2}]+v\frac{s}{(r^2+s^2)^{1/2}}\right]_0^{L/2} \tag{7}$$

Since $L \gg b$ and $-b \leqslant r \leqslant b$, then $L \gg r$. As a consequence, Eq. (7) becomes

$$2\int_0^{L/2}\left[\frac{(1-v)}{\sqrt{r^2+s^2}}+\frac{vr^2}{(r^2+s^2)^{3/2}}\right]\mathrm{d}s \cong 2\left[(1-v)\,\ln\left|\frac{L}{r}\right|+v\right] \tag{8}$$

and substituting it in Eq. (6), the final formulation is obtained:

$$u_x = -\frac{2(1-v^2)}{\pi E}\int_{-b}^{b} q_x(r)\,\ln\left|\frac{r}{b}\right|\mathrm{d}r+\frac{2(1-v^2)}{\pi E}\left(\ln\left|\frac{L}{b}\right|+\frac{v}{1-v}\right)\int_{-b}^{b} q_x(r)\,\mathrm{d}r \tag{9}$$

Since the second integral of Eq. (9) is the tangential force per unit length applied at the contact ($Q = T/L$), the final expression for relative tangential displacement between distant points in the two bodies is

$$\delta_x = u_{x1}-u_{x2} = \frac{2}{\pi E^*}\left[-\int_{-b}^{b} q_x(r)\,\ln\left|\frac{r}{b}\right|\mathrm{d}r+Q\left(\ln\left|\frac{L}{b}\right|+\frac{v}{1-v}\right)\right] \tag{10}$$

### 2.4. Hysteresis curves

Eq. (10) allows computing the monotonic loading curve of the tangential force $Q$ vs. the relative tangential displacement $\delta_x$ of contact bodies.

In order to compute the whole hysteresis loop in the microslip regime, that is for $Q/\mu P<1$ (Fig. 7a), from the monotonic curve, the Masing hypothesis [24,25] can be used.

The mathematical representation of this hypothesis can be expressed as

$$\delta_u(Q) = \delta^* - 2M\left(\frac{Q^*-Q}{2}\right) \tag{11}$$

which states that the unloading displacement, $\delta_u$, is given by the displacement at load reversal, $\delta^*$, minus twice the function, $M$, which relates displacement and force under the monotonic loading curve (i.e., Eq. (10)), evaluated for a tangential load equal to $(Q^*-Q)/2$. The reloading displacement, $\delta_r$, is the negative of the unloading displacement with a negative argument

$$\delta_r(Q) = -\delta_u(-Q) \tag{12}$$

By applying this method, it is clear that all properties of the hysteresis loop are embedded in the first loading curve.

Masing was the first to propose this approach to characterize hysteresis loop in elasto-plastic material, however this hypothesis has been applied in the field of friction contact modelling [30]. In order to check the validity of the Masing rule adopted in this paper, the hysteresis loops of tangential contact forces have been also computed by means of Eq. (10), using the shear stress distributions for oscillating tangential force [31], confirming that both the approaches lead to the same result. It can also be noted that by applying this simple and effective rule to the classical results obtained by Mindlin for spherical bodies in contact [17], it is possible to obtain the same equation for the unloading and reloading process derived by Mindlin et al. in Ref. [18].

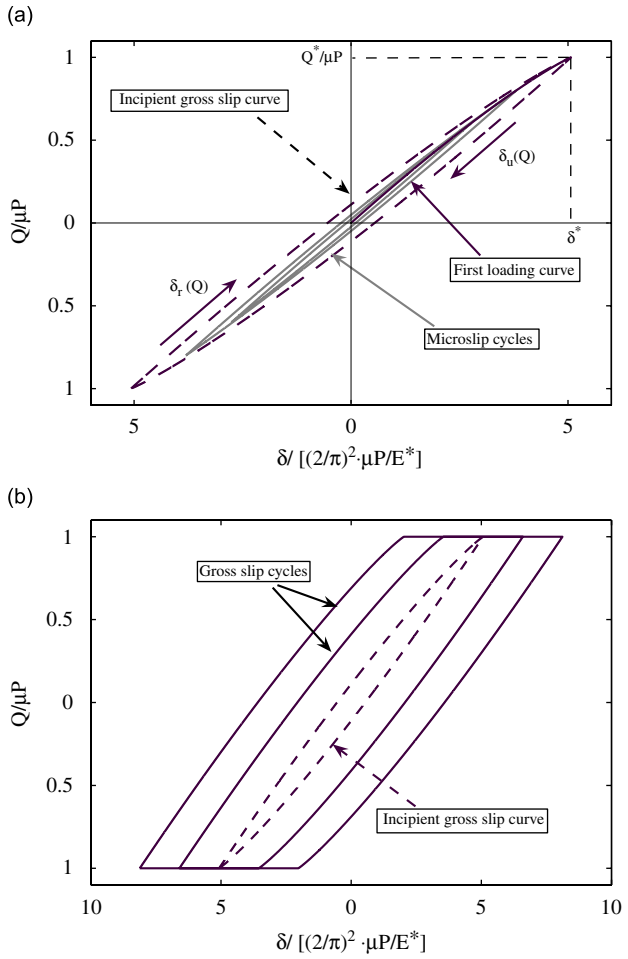


Fig. 7. (a) and (b) Hysteresis curves for different displacement amplitudes, microslip and gross-slip behaviour.

Curves in the gross-slip regime are easily obtained by extending horizontally the curve corresponding to the incipient gross slip ($Q/\mu P = 1$) as shown in Figs. 7a and b, where normalized tangential contact force and normalized relative displacement are plotted.

The proposed method provides the hysteresis curves as a quasi-static solution [32] of the contact problem, i.e., for a loading rate sufficiently slow that it is possible to define the curves as a sequence of equilibrium states. A model like that, obviously, does not predict any effect of the vibration frequency on the contact damping. However dry friction damping, in the typical range of frequency of turbine components, is normally considered frequency independent as it was experimentally verified in Ref. [10].

## 3. Results

In this part, the method described in Section 1, is applied to different contact geometries; hysteresis curves, complex contact stiffness and dissipated energy are provided and compared.

### 3.1. Hysteresis curves

The hysteresis curves obtained from Eq. (10), for the geometries under study, depend on the material properties ($E^*$,$v$) and on two parameters: the ratio $a/b$, that modifies the shear stress distribution $q(x)$ and the

ratio $L/b$. The first one affects the value of the integral in Eq. (10), while the second one affects the second part of the same equation.

In Fig. 8 two hysteresis curves for two different contact geometries are plotted. The first one, $a/b = 0.1$, corresponds to a geometry tending to the Hertzian cylindrical contact, while the second one, $a/b = 0.9$, corresponds to a geometry tending to the flat indenter with sharp edges.

In microslip conditions, the area enclosed in the hysteresis cycles increases as long as the value of the ratio $a/b$ decreases. As a consequence, for a given displacement amplitude, normal load and material, the maximum dissipated energy is obtained for the Hertzian cylindrical contact, $a/b = 0$. In the Hertzian case, as the tangential load increases, microslip can gradually extend to the whole contact area; on the contrary in the flat indenter with rounded edges indenter, microslip is confined in the rounded part of the punch, whose size decreases as the ratio $a/b$ increases.

In Fig. 8 the effect of the parameter $L/b$ over the hysteresis curve is plotted. The ratio $L/b$ only affects the slope of the hysteresis cycle, but not its area and the corresponding value of energy dissipated for unit of length. This feature can be deduced directly from Eq. (9). Indeed the second term in the equation is linear in $Q$, so this term does not produce any energy dissipation but it only changes the slope of the hysteresis loop. The amount of dissipated energy depends on the first term of Eq. (9), which takes into account the actual shear distribution on the contact area.

### 3.2. Contact stiffness

The hysteresis curve characterizes completely the dynamic behaviour of the contact, however it is useful to plot the value of the contact stiffness as a function of the normal load $P$ applied to the contact. These curves can be used to extract the correct value of tangential contact stiffness to be employed in the numerical solvers currently used to compute the forced response of frictionally damped turbine blades.

All curves in Fig. 9 show that the tangential contact stiffness increases for increasing normal load. Nevertheless this behaviour is more marked for the cylindrical Hertzian contact ($a/R = 0$). This is due to the fact that for a cylindrical Hertzian contact, the contact area increases significantly increasing the normal load, while for an almost-flat contact the contact area is barely affected by the value of the normal load (Fig. 10).

### 3.3. Comparison with elliptical Hertzian contact

It is interesting to compare the monotonic loading curve obtained for cylindrical Hertzian contact and for an elliptical Hertzian contact with the major axis equal to the length of the cylinder, $L$, and the minor semi axis equal to the half-width of the contact, $b$ (Fig. 11). For the elliptical Hertzian contact the solution is provided in close form in Ref. [33].

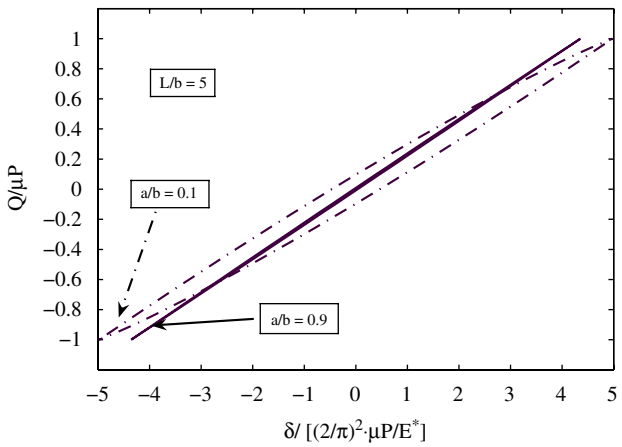


Fig. 8. Hysteresis curves for a given ratio $L/b$ and for two different values of the ratio $a/b$.

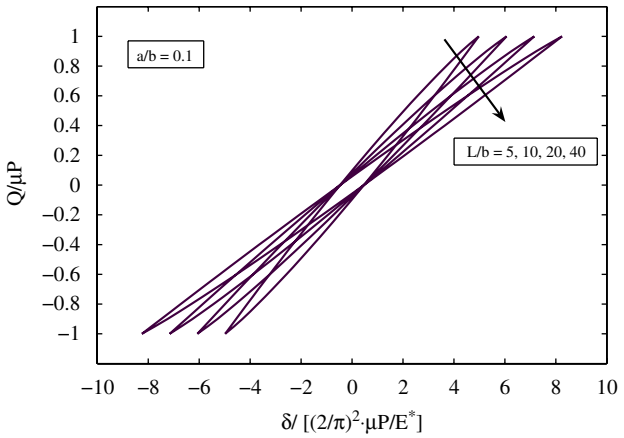


Fig. 9. Hysteresis curves for a given ratio $a/b$ and for different values of the ratio $L/b$: 5, 10, 20, 40.

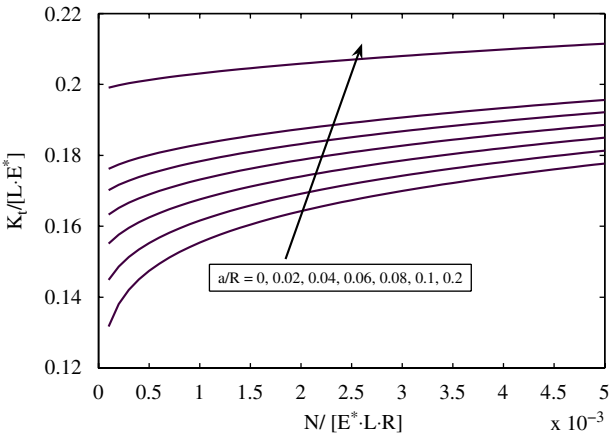


Fig. 10. Tangential contact stiffness vs. non-dimensional normal load. Different curves for a given ratio $L/r = 10$ and different ratios $a/R$.

It can be noted that the two curves plotted in Fig. 11 have a common tangent for vanishing relative displacement. This value is usually defined as the contact stiffness associated to the contact. This value corresponds to the value of the slope of the hysteresis curves plotted in Fig. 7 at the reversal of motion.

Comparing the areas under the two curves of Fig. 11 it is evident that more energy is dissipated in microslip regime by the elliptical contact. This feature can be explained by the fact that in the elliptical contact microslip, initiating at the outer edge, extends inward over an annular area and at the microslip–gross-slip transition theoretically only one point in the contact area is in stick condition, so that the transition is very smooth and the hysteresis curve has a horizontal tangent. Differently for the cylindrical contact, under the assumption here proposed, the microslip can penetrate only in two bands at the outer edges of the contact (Fig. 12) and at the transition between microslip and gross-slip regime, there is a line of points in the stick condition yet.

### 3.4. Harmonic contact stiffness

As it was highlighted in the Introduction the steady-state dynamic response of structures embedding friction contacts is commonly performed by means of the harmonic balance method [34]. The response of the structure is assumed to be harmonic or a superimposition of harmonics. However in many cases only the principal harmonic is adopted. Using the rotating vector notation, the first harmonic component of the tangential contact force is a complex number representing the harmonic equivalent contact force, whose real part is

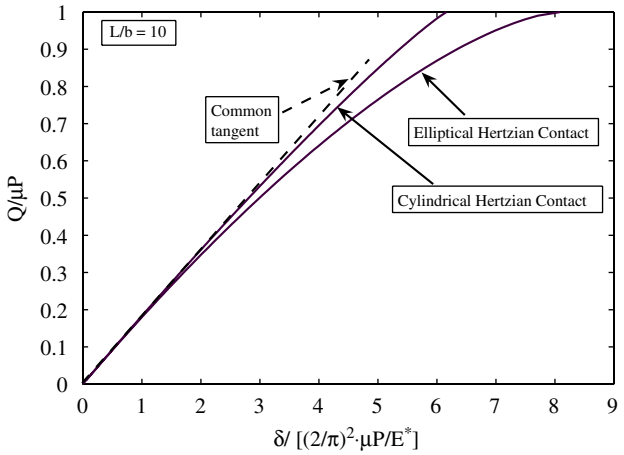


Fig. 11. First loading curve for a cylindrical Hertzian contact and for an elliptical Hertzian contact.

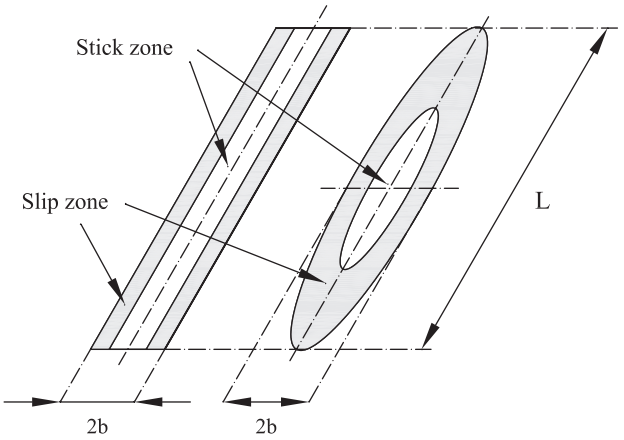


Fig. 12. Contact area for a cylindrical Hertzian contact and for an elliptical Hertzian contact.

the component in phase with the displacement and the imaginary part is the out of phase component. This equivalent force divided by the amplitude of relative displacement provides a complex number: the harmonic contact stiffness. The real part of the harmonic contact stiffness affects the resonance frequencies of the system but does not produce any energy dissipation. The imaginary part represents an equivalent damping, it affects the resonance response amplitudes but does not affect the resonant frequencies. These two components of the harmonic contact stiffness effectively summarize the whole contact hysteresis and can be easily obtained from the hysteresis curves [10].

In Figs. 13 and 14 the real and the imaginary part of the contact stiffness for unit of length for the hysteresis curves previously obtained are plotted.

In microslip conditions, the imaginary part of the complex contact stiffness increases larger for small values of the $a/b$ ratio, on the contrary for ratio $a/b$ tending to unity the energy dissipated in the microslip is almost null and the value of the imaginary part of the contact stiffness does not increase significantly before the microslip–gross-slip transition. In Ref. [31] it is shown that, for a perfect flat indenter, microslip does not occur. However it is important to keep in mind that the more the ratio $a/b$ tends to the unity the weaker the assumption of half-plane becomes. All the curves of the real part of the complex contact stiffness start from the same value. This confirms the assertion previously made that the initial slope of the first loading curve depends basically on the ratio $L/b$ and not on the particular shape of the contact bodies.

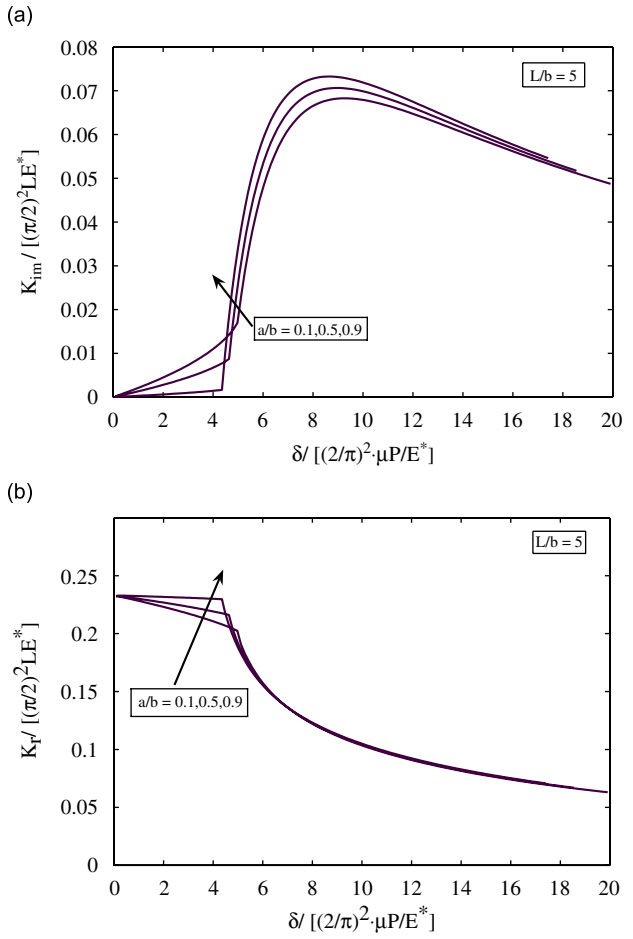


Fig. 13. Imaginary (a) and real (b) part of the complex contact stiffness for a given ratio $L/b$. Different curves for different values of the ratio $a/b$.

In Fig. 14, the harmonic contact stiffness is plotted for different values of the $L/b$ ratio. It is worth noting that the starting value of the real contact stiffness decreases as the ratio $L/b$ increases. If this ratio would tend to infinity the value of the stiffness would tend to zero. This feature is consistent with a 2D contact problem where for assumption $L/b \to \infty$ and, as it was pointed out in the Introduction, the displacement of a point distant from the contact tends to infinity.

### 3.5. Energy dissipation

As a further result of this work, the curves of the energy dissipated as function of the ratio $Q/\mu P$ are provided. Several numerical works [35–37], focused on the effect of mechanical joints on the damping capability of the structures, remark that the energy expended on contact in the microslip regime is proportional to the cube of applied the tangential force and the same proportionality was obtained by Mindlin [17] for the contact of two elastic spheres under a cyclic tangential load. Also experimental results confirm the power–law relationship between dissipated energy and tangential load, even if the power–law exponent obtained from experimental data is not unanimously 3 but ranges between 2.0 and 3.33 [38–42]. As it is pointed out by a reviewer this can depend on the roughness and waviness of the surface texture as well as on the applied normal load. The Greenwood–Tripp model [43] can explain this behaviour. Numerical models neglecting roughness, as the one presented in this paper, can be thought of as the limiting case to which real contacts tend as the surfaces become ideally smooth. A selected literature that deals with the

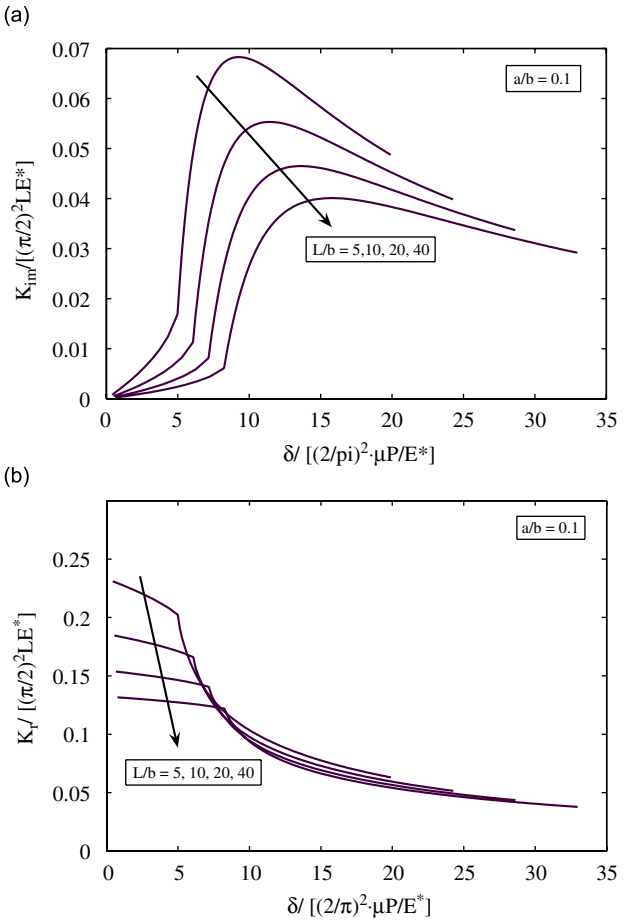


Fig. 14. Imaginary (a) and real (b) part of the complex contact stiffness for a given ratio $a/b$. Different curves for different values of the ratio $L/b$.

subject to describe the effect of roughness on the contact behaviour is suggested to the author by one of the reviewers [44–46].

As shown in Fig. 15, also the contact model here developed predicts a power-law behaviour. All the different curves, for different values of the ratio $a/b$, if plotted in logarithmic scale, are approximately straight lines with a slope, tg(α), equal to 3, denoting the cube proportionality.

The same curves plotted in Fig. 15 could be computed by means of the 2D contact problem assumptions without using the 3D contact formulation. If the shear stress distributions, $q_x(x)$, and the slip amplitude of relative points in the contact area, $s_x(x)$, are known for the first loading process, the dissipated energy in microslip regime can be evaluated by integration of the infinitesimal work at the surface (Eq. (13)). The energy dissipated per cycle will be four time the energy dissipated as the load increases from zero to its maximum value:

$$E = 4 \cdot L \cdot \int_{L_{\mathrm{SLIP}}} s_x(x) \cdot q_x(x)\,\mathrm{d}x \tag{13}$$

By noting that in the slip region $q_x(x) = \mu p(x)$, Eq. (13) may be written as

$$E = 4 \cdot L \cdot \int_{L_{\mathrm{SLIP}}} s_x(x) \cdot \mu p(x)\,\mathrm{d}x \tag{14}$$

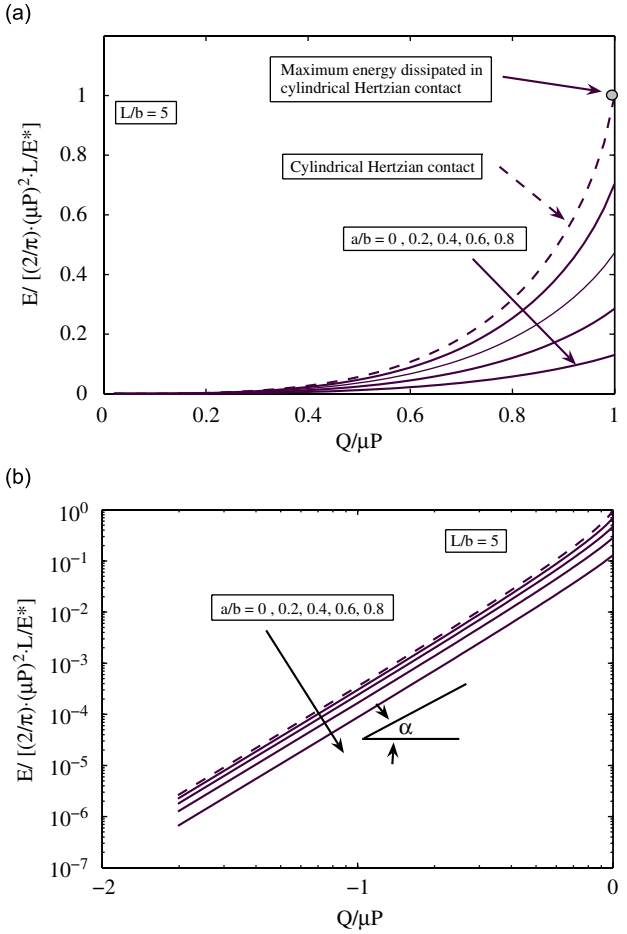


Fig. 15. Energy dissipated in the microslip regime ($Q/\mu N \leqslant 1$). Linear (a) and logarithmic (b) diagram.

where the argument of the integral in Eq. (14), $s_x(x) = \mu p(x)$, is commonly defined frictional damage parameter, $D(x)$, and it is utilized by many authors [31,47] to quantify the effect of fretting on surfaces.

If the two bodies have the same material properties, $E$ and $v$, the relative slip at the contact is

$$s(x) = -2\frac{2(1-v^2)}{\pi E}\int_{-b}^{a} q(r)\,\ln|x-r|\,\mathrm{d}r + C_1 \tag{15}$$

To eliminate the constant $C_1$ is sufficient to impose that slip vanishes in the stick zone, i.e., $s(|x| \leqslant c) = 0$, where $c$ is the limit of the stick zone. For example it could be useful to impose that $s(x)$ vanishes at the origin ($x = 0$).

Typically the integral in Eq. (15) must be evaluated numerically, however for the cylindrical indenter, knowing the relative displacement at the contact in close form [48], it is possible to evaluate the integral analytically in the case of incipient sliding and to obtain

$$\frac{E_{\mathrm{Lim}}}{\dfrac{2(\mu P)^2 L}{\pi \quad E^*}} = 1 \tag{16}$$

This value is marked by a circle in Fig. 15.

## 4. Conclusions

In this paper a model to characterize cylindrical and flat friction contacts in case of 1D relative tangential kinematics under both microslip and macroslip conditions is presented. The method can be applied when the contact area is rectangular and characterized by a large aspect ratio (i.e. contact length much larger than contact width).

By means of the proposed method it is possible to compute:

1. hysteresis cycles of tangential contact force vs. the relative tangential displacement,
2. tangential contact stiffness,
3. energy dissipated at the contact interface.

The main geometrical parameters of the contact model have been highlighted and their effects over the resulting hysteresis cycles and contact stiffness have been discussed.

Real and imaginary terms of the harmonic contact stiffness, usually used to characterize in dynamics the behaviour of friction contacts, have been computed and analysed for different contact geometries.

The hysteresis curves obtained with the proposed model are suitable to be implemented in numerical solvers for the forced response calculation of turbine bladed discs with friction interfaces such as blade roots, shrouds and underplatform dampers. If variation of the contact normal load is negligible during vibration, the complex contact stiffness as function of the relative displacement can be directly introduced in the non-linear dynamic model of the structure, otherwise this work provides the stiffness parameters necessary to the contact model commonly employed to compute the forced response of turbine blades with friction contacts.

### Acknowledgements

The author wishes to acknowledge all the help provided by Dr. Stefano Zucca and Prof. Muzio Gola.

### Appendix A. Pressure and shear traction distributions

In this appendix are reported the equations used to obtain the graph in Figs. 3 and 4, more details in Ref. [22].

The normal pressure distribution is provided by the following equations:

$$\frac{bp(\varphi)}{P} = \underbrace{\frac{2/\pi}{\pi - 2\varphi_0 - \sin 2\varphi_0}\left\{(\pi - 2\varphi_0)\cos(\varphi) + \ln\left[\left|\frac{\sin(\varphi+\varphi_0)}{\sin(\varphi-\varphi_0)}\right|^{\sin\varphi}\left|\tan\frac{\varphi+\varphi_0}{2}\tan\frac{\varphi-\varphi_0}{2}\right|^{\sin\varphi_0}\right]\right\}}_{f(\varphi,\varphi_0)} \tag{17}$$

where

$$\sin(\varphi) = \frac{x}{b} \tag{18}$$

and $b$ is the half-width of the contact area.

The angle $\varphi_0$, and therefore the size of the contact area, may be found using the following implicit equation:

$$\frac{4PR}{a^2E^*} = \frac{\pi - 2\varphi_0}{2\sin^2\varphi_0} - \cot(\varphi_0) \tag{19}$$

where

$$\sin(\varphi_0) = \frac{a}{b} \tag{20}$$

It is possible to write the tangential traction like a superimposition of two functions

$$q(x) = \mu p(x) - q^*(x) = \mu(p(x) - p^*(x)) \tag{21}$$

It can be shown that for two arbitrary bodies in contact the tangential traction distribution is equal to the difference between the actual pressure distribution, $p(x)$, and the pressure distribution for a smaller contact area, $p^*(x)$, multiplied by the coefficient of friction, $\mu$.

The expression for $q^*$ is similar to the one for $p(\varphi)$.

$$\frac{cq^*(\vartheta)}{\mu P - Q} = -\underbrace{\frac{2/\pi}{\pi - 2\vartheta_0 - \sin 2\vartheta_0}\left\{(\pi - 2\vartheta_0)\cos(\vartheta) + \ln\left[\left|\frac{\sin(\vartheta+\vartheta_0)}{\sin(\vartheta-\vartheta_0)}\right|^{\sin\vartheta}\left|\tan\frac{\vartheta+\vartheta_0}{2}\tan\frac{\vartheta-\vartheta_0}{2}\right|^{\sin\vartheta_0}\right]\right\}}_{f(\vartheta,\vartheta_0)} \tag{22}$$

where

$$\sin(\vartheta_0) = \frac{a}{c} \tag{23}$$

may be found using

$$\frac{4PR}{a^2E^*}\left(1 - \frac{Q}{\mu P}\right) = \frac{\pi - 2\vartheta_0}{2\sin^2\vartheta_0} - \cot(\vartheta_0) \tag{24}$$

## References


[1] J.H. Griffin, Friction damping of resonant stresses in gas turbine engine airfoils, *Transaction of the American Society of Mechanical Engineers, Journal of Engineering for Power* 102 (1980) 329–333.

[2] C.H. Menq, J. Bielak, J.H. Griffin, The influence of microslip on vibratory response, part I: a new microslip model, *Journal of Sound and Vibration* 107 (1986) 279–293.

[3] C.H. Menq, J. Bielak, J.H. Griffin, The influence of microslip on vibratory response, part II: a comparison with experimental result, *Journal of Sound and Vibration* 107 (1986) 295–307.

[4] E.P. Petrov, D.J. Ewins, Analytical formulation of friction interface elements for analysis of nonlinear multiharmonic vibrations of bladed discs, *Transaction of the American Society of Mechanical Engineers, Journal of Turbomachinery* 125 (2003) 364–371.

[5] S. Zucca, J. Borrajo, M.M. Gola, Forced response of bladed disks in cyclic symmetry with underplatform dampers, *Proceedings of the ASME Turbo Expo GT2006*, Barcelona, Spain, 2006.

[6] C.M. Firrone, D. Botto, M.M. Gola, Modelling a friction damper: analysis of the experimental data and comparison with numerical results, *Proceedings of Eighth Biennial ASME Conference ESDA*, Turin, Italy, 2006.

[7] E. Cigeroglu, W. Lu, C.H. Menq, One-dimensional dynamic microslip friction model, *Journal of Sound and Vibration* 292 (2006) 881–898.

[8] B.D. Yang, M.L. Chu, C.H. Menq, Stick–slip separation analysis and non-linear stiffness and damping characterization of friction contacts having variable normal load, *Journal of Sound and Vibration* 210 (1998) 461–481.

[9] E.P. Petrov, D.J. Ewins, Analytical formulation of friction interface for analysis of nonlinear multi-harmonic vibrations of bladed discs, *Proceedings of the ASME Turbo Expo GT2002*, Amsterdam, The Netherlands, 2002.

[10] S. Filippi, A. Akay, M.M. Gola, Measurement of tangential contact hysteresis during microslip, *Transaction of the American Society of Mechanical Engineers, Journal of Tribology* 126 (2004) 482–489.

[11] E.P. Kingsbury, E. Rabinowicz, Friction and wear of metals to 1000 C, *Transaction of the American Society of Mechanical Engineers* 81D (1959) 118–121.

[12] S. Filippi, E.B. Rodrigues, M.M. Gola, Experimental characterization of contact hysteresis at high temperatures, *Proceedings of the ASME Turbo Expo GT2006*, Barcelona, Spain, 2006.

[13] A.B. Stanbridge, D.J. Ewins, K.Y. Sanliturk, J.V. Ferreira, Experimental investigation of dry friction damping and cubic stiffness non-linearity, *Proceedings of the ASME Design Engineering Technical Conference*, Pittsburgh, PA, USA, 2001.

[14] J. Szwedowicz, M. Kissel, B. Ravindra, R. Kellerer, Estimation of contact stiffness and its role in the design of a friction damper, *International Gas Turbine and Aeroengine Congress*, New Orleans, LA, USA, 2001.

[15] C. Siewert, L. Panning, A. Schmidt-Fellner, A. Kayser, The estimation of the contact stiffness for directly and indirectly coupled turbine blading, *Proceedings of the ASME Turbo Expo GT2006*, Barcelona, Spain, 2006.

[16] U. Sellgren, U. Olofsson, Application of constitutive model for micro-slip in finite element analysis, *Computer Methods in Applied Mechanics and Engineering* 170 (1999) 65–77.

[17] R.D. Mindlin, Compliance of elastic bodies in contact, *Journal of Applied Mechanics* 16 (1949) 259–268.

[18] R.D. Mindlin, W.P. Mason, T.F. Osmer, H. Deresiewicz, Effects of an oscillating tangential force on the contact surfaces of elastic spheres, *Proceedings of the First US National Congress of Applied Mechanics*, 1952, pp. 203–208.

[19] K.H. Koh, J.H. Griffin, S. Filippi, A. Akay, Characterization of turbine blade friction dampers, *ASME Journal of Engineering for Gas Turbines and Power* 12 (2005).

[20] K.-H. Koh, J.H. Griffin, Dynamic behaviour of spherical friction dampers and its implication to damper contact stiffness, *Proceedings of the ASME Turbo Expo GT2006*, Barcelona, Spain, 2006.
[21] K.L. Johnson, *Contact Mechanics*, Cambridge University Press, Cambridge, 1985.
[22] M. Ciavarella, D.A. Hills, G. Monno, The influence of rounded edges on the indentation by a flat punch, *Proceedings of the Institution of Mechanical Engineers* 212 (1998) 319–328.
[23] A.E.H. Love, *Tractise of Mathematical Theory of Elasticity*, Cambridge University Press, Cambridge, 1927.
[24] G. Masing, Eigenspannungen und verfestigung beim messing, *Proceedings of the Second International Congress Applied Mechanics*, 1926, pp. 332–335 (in German).
[25] D.J. Segalman, M.J. Starr, Inversion of Masing models via continuous Iwan systems, *Non Linear Mechanics* 43 (2008) 74–80.
[26] J. Jäger, A new principle in contact mechanics, *Journal of Tribology* 120 (1999) 677–684.
[27] M. Ciavarella, D.A. Hills, A note on convective effect in elastic contact problems for dissimilar materials, *European Journal Mechanics A/Solids* 18 (3) (1999) 481–490.
[28] D.A. Hills, D. Nowell, A. Sackfield, *Mechanics of Elastic Contacts*, Butterworth-Heinemann, Oxford, 1993.
[29] M. Ciavarella, Indentation by nominally flat or conical indenters with rounded corners, *International Journal of Solids and Structures* 36 (1999) 4149–4181.
[30] A.B. Stanbridge, K.J. Sanliturk, D.J. Ewins, Measurement and analysis of height–temperature friction damper properties, *Proceedings of the Fourth National Turbine Engine High Cycle Fatigue* (*HCF*) *Conference*, 1999.
[31] M. Ciavarella, G. Demelio, A review of analytical aspects of fretting fatigue with extension to damage parameters and application to dovetail joints, *International Journal of Solids and Structures* 38 (2001) 1791–1811.
[32] J.R. Barber, M. Ciavarella, Contact mechanics, *International Journal of Solids and Structures* 37 (2000) 29–43.
[33] H. Deresiewicz, Oblique contact of nonspherical elastic bodies, *Journal of Applied Mechanics* 24 (4) (1957) 623–624.
[34] K.Y. Sanliturk, D.J. Ewins, Modeling two-dimensional friction contact and its application using harmonic balance method, *Journal of Sound and Vibration* 193 (1996) 511–523.
[35] L.E. Goodman, J.H. Klumpp, Analysis of slip damping with reference to turbine-blade vibration, *Journal of Applied Mechanics* 23 (1956) 421–429.
[36] A.F. Metherell, S.V. Diller, Instantaneous energy dissipation rate in a lap joint—uniform clamping pressure, *Journal of Applied Mechanics* 35 (1968) 333–340.
[37] W. Chen, X. Deng, Structural damping caused by micro-slip along frictional interfaces, *International Journal of Mechanical Sciences* 47 (2005) 1191–1211.
[38] K. Johnson, Surface interaction between elastically loaded bodies under tangential and forces, *Proceedings of the Royal Society A* 230 (1955) 531–548.
[39] R.V. Klint, Oscillating tangential forces on cylindrical specimens in contact transmitting oscillating forces, *Journal of Mechanical Engineering Sciences* 3 (4) (1962) 362–368.
[40] I.V. Kragelsky, M.N. Dobychin, V.S. Kombalov, *Friction and Wear: Calculation Methods*, Pergamon Press, Oxford, 1982.
[41] D.O. Smallwood, D.L. Gregory, R.G. Coleman, Damping identification of a simplified frictional shear joint, *Proceedings of 71st Shock and Vibration Symposium*, Arlington, VA, USA, 2000.
[42] C.J. Hartwigsen, Y. Song, D.M. McFarland, L.A. Bergman, A.F. Vakakis, Experimental study of non-linear effects in a typical shear lap joint configuration, *Journal of Sound and Vibration* 277 (2004) 327–351.
[43] J.A. Greenwood, J.H. Tripp, The elastic contact of rough spheres, *Journal of Applied Mechanics* 34 (1967) 153–159.
[44] S. Björklund, A random model for micro-slip between nominally flat surfaces, *Journal of Tribology* 119 (1997) 726–732.
[45] U. Olofsson, L. Hagman, A model for micro-slip between flat surfaces based on deformation of ellipsoidal elastic bodies, *Tribology International* 30 (1997) 599–603.
[46] Yu.A. Karpenko, A. Akay, A numerical method for analysis of extended rough wavy surfaces in contact, *Journal of Tribology* 124 (2002) 668–679.
[47] D. Nowell, D.A. Hills, Crack initiation criteria in fretting fatigue, *Wear* 136 (1990) 329–343.
[48] H. Poritsky, N.Y. Schenectady, Stresses and deflection of cylindrical bodies in contact with application to contact gears and locomotive wheels, *Journal of Applied Mechanics* 17 (1950) 191–201.